Geological Society of America
Special Paper 356
2002

Generation and propagation of a tsunami from the Cretaceous-Tertiary impact event

T. Matsui*
Department of Complexity Science and Engineering, Graduate School of Frontier Science, University of Tokyo, 7-3-1 Hongo, Bunkyo-ku, Tokyo 113-0031, Japan
F. Imamura*
Disaster Control Research Center, Graduate School of Engineering, Tohoku University, Aoba 06, Sendai 980-8579, Japan
E. Tajika*
Y. Nakano*
Department of Earth and Planetary Science, Graduate School of Science, University of Tokyo, 7-3-1 Hongo, Bunkyo-ku, Tokyo 113-0031, Japan
Y. Fujisawa*
Technical Research Institute, Obayashi Corporation, Shimo-kiyose 4-640, Kiyose 204-0011, Tokyo, Japan

ABSTRACT

We have studied mechanism of tsunami generation by meteorite impact on a shallow ocean at 65 Ma and modeled the propagation of that tsunami in the Gulf of Mexico. We found that the water flow into and out of the crater cavity causes most of the tsunami. The height of the wave coming out of the crater is controlled by the depth of the shallow-water region surrounding the crater. We show that the lower the flow velocity in the shallow-water region, the lower the wave height, and the longer the oscillation period. If the depth of the sea above the Yucatan platform was 200 m at the end of the Maastrichtian, the maximum tsunami wave height and period at the rim of the crater are estimated to be ~50 m and 10 h, respectively.

Using these results, we simulated the propagation of the K-T impact-generated tsunami in the Gulf of Mexico. There are two types of tsunami; the receding wave and the rushing wave. The receding wave traveled across the entire gulf within 10 h of the impact. Tsunamis attacked the coast as a leading negative wave. The rushing wave flowed with a height of more than 200 m and reached the coastal area of North America. It ran up over the land and crossed the Mississippi embayment, a distance of more than 300 km. The averaged runup was more than 150 m, but it reached a height of 300 m near the Rio Grande embayment.

*E-mails: Matsui, matsui@k.u-tokyo.ac.jp; Imamura, imamura@tsunami2.civil.tohoku.ac.jp; Tajika, tajika@eps.s.u-tokyo.ac.jp; Nakano, nakano@sys.eps.s.u-tokyo.ac.jp; Fujisawa, Fujisawa@tri.obayashi.co.jp

Matsui, T., Imamura, F., Tajika, E., Nakano, Y., and Fujisawa, Y., 2002, Generation and propagation of a tsunami from the Cretaceous-Tertiary impact event, *in* Koeberl, C., and MacLeod, K.G., eds., Catastrophic Events and Mass Extinctions: Impacts and Beyond: Boulder, Colorado, Geological Society of America Special Paper 356, p. 69–77.

INTRODUCTION

A gigantic meteorite impact occurred at the Yucatan Peninsula ca. 65 Ma and resulted in the formation of the Chicxulub crater (e.g., Hildebrand et al., 1991); hereafter, we call this the K-T (Cretaceous-Tertiary) impact event. After the discovery of the Chicxulub crater on the Yucatan Peninsula (Hildebrand et al., 1991), studies of the K-T impact event focused on the environmental consequences of this gigantic meteorite impact. One example of such studies concerns the K-T boundary tsunami deposits found in and around the Gulf of Mexico (e.g., Bourgeois et al., 1988; Smit et al., 1996), although their origin is still controversial (e.g., Bohor, 1996). A Japanese-Cuban joint research group reported the discovery of an ~180-m-thick layer, which consists of a lower grain flow unit overlain by an upper homogenite unit, the age of which is definitively defined as that of the K-T boundary (Takayama et al., 2000). The homogenite is a thick, normally graded, but otherwise structureless deposit formed by a tsunami in a deep-sea environment (Cita et al., 1996). This discovery supports tsunami generation by the K-T impact.

There are some studies on numerical simulation of a tsunami caused by a small asteroid impact into deep water (e.g., Hills et al., 1994; Crawford and Mader, 1998; Ward and Asphaug, 2000). There has been, however, no study of a tsunami generated by a large asteroid impact into shallow water, as in the case of the K-T impact. Here, we study the generation mechanism of the K-T impact tsunami and its propagation within the Gulf of Mexico.

MODEL

Tsunami generation

The diameter of the impactor that formed the Chicxulub crater has been estimated as ~10 km, based on the total amount of Ir in the K-T boundary layer (Alvarez et al., 1980). The energy released by a 10 km meteorite impact with a velocity of several tens of kilometers/second on the Earth would correspond to a TNT explosion energy of 10^8 to 10^9 Mt. The diameter and depth of the crater formed by this impact are ~180 km and several kilometers, respectively (Morgan et al., 1997; Hildebrand et al., 1998).

In association with this impact, shock waves would have propagated through the atmosphere, ocean, crust, and mantle, and both the seawater and seafloor at the impact point would have been vaporized instantaneously. Shock waves caused by the entry of the meteorite into the atmosphere and ejecta from the crater could have both induced tsunamis. Hereafter we refer to the first of these as the shock-wave-induced tsunami and to the second, i.e., the wave formed at the front of the ejecta curtain, as the rim wave. According to Gault and Sonett (1982), the rim wave is generated and propagates away from the cavity as shown in Figure 1. As a more gradual process, the surrounding seawater may have flowed back into the crater. Then the crater would have been overfilled with water, and a central water column would form above the crater. The height of the water column would be dependent on the depth of the ocean around the crater, because the flow rate of water into the crater from the surrounding ocean is controlled by the water depth. The elevated water column would then collapse and could eventually propagate outward from the crater site as a tsunami.

We also expect the formation of landslides at the margin of the Yucatan platform. The basal unit of the type locality for the Peñalver Formation in Cuba is several tens of meters thick and shows features characteristic of a sediment gravity flow (Takyama et al., 2000). Such gravity flow units are common for the Peñalver Formation at other localities and for the Cacarajicara Formation in Cuba (Kiyokawa et al., 2000). These observations suggest that large-scale landslides occurred at the margin of the Yucatan platform just after the K-T impact.

We consider four stages of tsunami generation by the K-T impact: (1) the shock-wave-induced tsunami associated with high air pressure and wind generated by the passage of the meteorite through the atmosphere, (2) the rim wave formed at the front of the ejecta curtain, (3) the crater-generated tsunami, caused by movement of water to fill and flow out of the crater cavity after crater formation (hereafter called receding and rushing waves, respectively), and (4) the landslide-generated tsu-

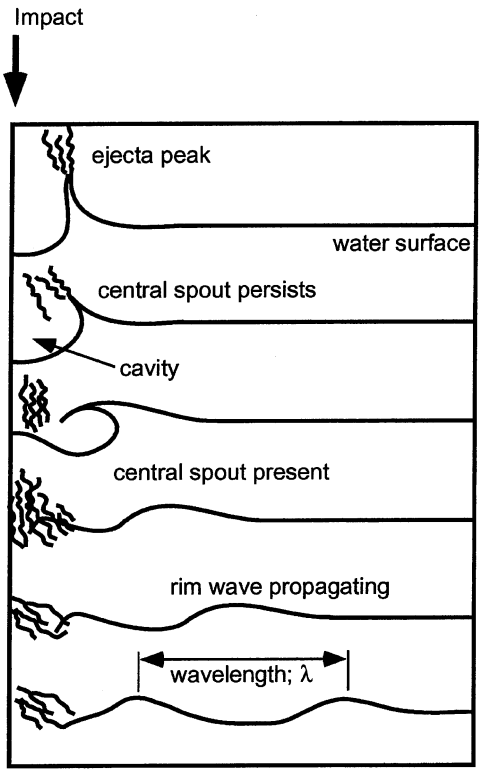

Figure 1. Wave formation sequence in case of impact into shallow water (modified from Gault and Sonett, 1982). Rim wave is generated and propagated away from cavity.

nami, caused by landslides at the margin of the Yucatan platform. The wave generation by the first mechanism is negligible, because waves generated by strong winds are dispersive and rapidly damped during propagation over a long distance. Waves generated by the second mechanism were modeled as the initial condition of the rim wave, wave height and length being estimated using the hydraulic experimental results of Gault and Sonett (1982). Waves generated by the third and fourth mechanisms might have been the most devastating, and were simulated based on shallow-water (nonlinear long wave) theory.

Paleobathymetry

In order to simulate tsunami generation and propagation due to the K-T impact, we assumed a probable paleobathymetry of the region at the time of the K-T impact. As shown herein, the shape of the crater does not have a significant effect on the generation and propagation of tsunami. Hence, we simply assume that the crater shape just after the impact was almost like the present shape of the Chicxulub crater (e.g., Morgan et al., 1997; Hildebrand, 1997). We also assume that the Yucatan Peninsula was covered with shallow water (<200 m deep) at the end of the Maastrichtian (Sohl et al., 1991). For the reconstruction of paleobathymetry of the Gulf of Mexico and the Caribbean region, we adopted the tectonic reconstruction model by Ross and Scotese (1988), modified slightly based on the field work in Cuba by Takayama et al. (2000). In Figure 2 we show the reconstructed ocean-floor geometry in the Gulf of Mexico (after Ross and Scotese, 1988) and the location of the Chicxulub crater. A cross section along the line A-A′ in Figure 2 is shown in Figure 3.

NUMERICAL PROCEDURE

We used the nonlinear long-wave theory (e.g., Imamura, 1996) to simulate the movement of water on the Yucatan platform and in the Gulf of Mexico. In this section we describe briefly the basic equations and numerical procedures used in this study.

Equations for tsunami generation and propagation

We applied the nonlinear long-wave theory integrated over a layer with nonhorizontal bottom and interface as the governing equation for the numerical model. We assume hydrostatic pressure distribution, and uniform density and velocity distributions in each layer. For tsunami generation by landslide, the seawater is modeled as an upper layer for wave generation and propagation, and the landslide is modeled as a lower layer in Figure 4. The Navier-Stokes equations of mass and momentum continuity are integrated in each layer, with the kinetic and dynamic conditions at a free surface and an interface (Imamura and Imteaz, 1995).

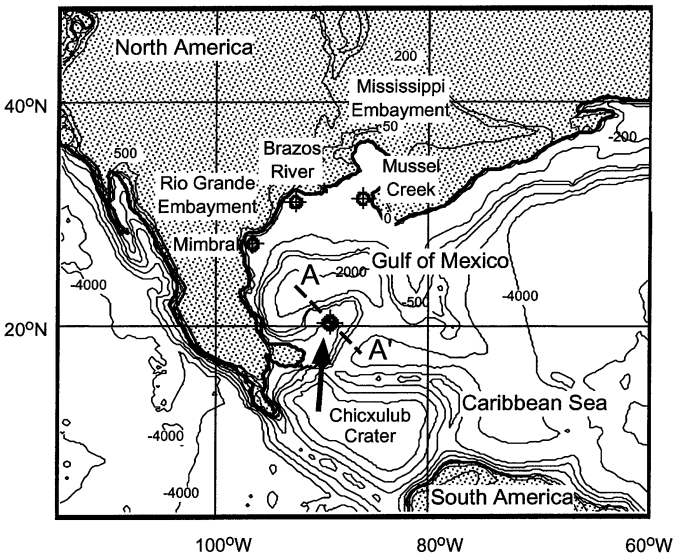

Figure 2. Reconstructed geometry of Gulf of Mexico at time of Cretaceous-Tertiary (K-T) impact, based on model by Ross and Scotese (1988). Locations of Chicxulub crater and some possible K-T boundary tsunami deposits around Gulf of Mexico are also shown.

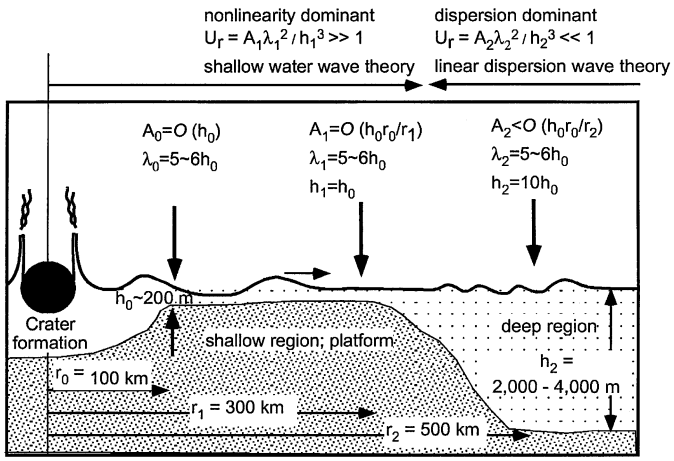

Figure 3. Cross section of topography of Chicxulub crater and Yucatan platform along line A-A′ in Figure 2. Schematic view of propagation of rim wave in near and far field and order estimate of wave amplitude are also shown. *A*, λ, *h*, *r*, and Ur represent amplitude, wavelength, depth, distance, and Ursell parameter, respectively.

The governing equations of the upper layer for a one-dimensional problem are expressed as follows. The equation of the mass conservation is given by:

$$\frac{\partial(\eta_1 - \eta_2)}{\partial t} + \frac{\partial M_1}{\partial x} = 0, \qquad (1)$$

where x is the horizontal coordinate, t is time, η_1 is the difference between the water surface and the still water depth, η_2 is the vertical displacement of the bottom, and subscripts 1 and 2 indicate the upper and lower layers, respectively (for details,

see Fig. 4). M is the discharge in the x direction given by the integration of velocity over a layer, which is defined by:

$$M = \int_{-h}^{\eta} u dz. \tag{2}$$

The momentum equation is given by:

$$\frac{\partial M_1}{\partial t} + \frac{\partial}{\partial x}\left(\frac{M_2^1}{D_1}\right) + gD_1\frac{\partial \eta_1}{\partial x} - L_x = 0, \tag{3}$$

where Lx is the drag force induced by a lower layer at the flow front, and is defined by:

$$L_x = \frac{1}{2} C_D \frac{1}{h}\frac{A_z}{A_c}\left(\frac{M}{D} - V\right)\left|\frac{M}{D} - V\right|, \tag{4}$$

where D is the total depth ($= h + \eta$), h is the still water depth, AZ is the projecting area of a lower layer flow at the flow front, Ac is the grid cell area of the water at the flow front, CD is the drag-force coefficient (as proposed by Raney and Bulter, 1976), and V is the velocity of sea-bottom displacement.

Landslide in a lower layer

We can assume two stages for a landslide; slumping and debris flows. The first stage, slumping, is modeled by a circular arc failure along a shear plane, similar to the model by Okusa and Yoshimura (1981) for displacement of the sea bottom under an oceanic wave. There are two types of slumping, toe slip and base slip. It is usually assumed that the surface of failure has a circular arc profile for both types (Imamura and Gica, 1996). In this study we use base slip for the surface of failure. Initiation of motion occurs when a sudden ground quake or external disturbance alters the balance of the internal resisting force and driving force. For the case of base slip, we can neglect the resisting force. If these conditions are satisfied, the tongue at the front of a landslide would start to move and flow down to the slope.

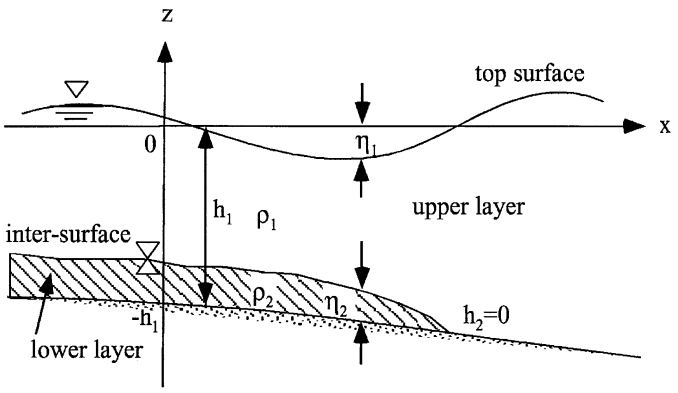

Figure 4. Two-layer model for movement of water and landslide (see text for discussion).

When landslide acceleration becomes negligibly small, debris flows become important. We use a different model of a lower layer for this stage. Here, the mass conservation equation for the lower layer is given by:

$$\frac{\partial \eta_2}{\partial t} + \frac{\partial M_2}{\partial x} = 0, \tag{5}$$

and the momentum equation becomes

$$\frac{\partial M_2}{\partial t} + \frac{\partial}{\partial x}\left(\frac{M_2^2}{D_2}\right) + gh_2\left\{\alpha\left(\frac{\partial \eta_1}{\partial x} + \frac{\partial h_1}{\partial x} - \frac{\partial \eta_2}{\partial x}\right) + \frac{\partial \eta_2}{\partial x} - \frac{\partial h_1}{\partial x}\right\} + g\eta_2(\alpha - 1)\frac{\partial h_1}{\partial x} + R_x + L_x = 0, \tag{6}$$

where

$$R_x = \frac{g\left(\frac{M}{D} - V\right)\left|\frac{M}{D} - V\right|}{C^2(h + \eta)}, \tag{7}$$

wherein ρ is the fluid density, $\alpha = \rho_1/\rho_2$, Rx is the bottom friction, and C is Chezy's roughness coefficient; other variables are as described for equations 3 and 4.

In addition, we considered two nonlinear interactions between the upper and lower layers. One is a change of η_1 due to η_2 in equation 1 for the upper layer. The other is a gravitational force caused by the upper layer, which affects the lower layer (see equation 6).

Numerical scheme and computational condition

We used the staggered leap-frog scheme for the linear terms and the up-wind scheme for the nonlinear terms in this study. The leap-frog scheme is a central difference scheme with a truncation error of the second order. In order to set the boundary conditions easily, the leap-frog scheme assumes that the computation point for the water surface does not coincide with the point for discharge and is therefore shifted by a half-time step and spatial grid. This is called the staggered scheme. Although the accuracy of the up-wind difference scheme is lower than that of the leap-frog scheme, we used it to make the computation stable for nonlinear terms. By using these schemes, we can resolve the water surface and discharge in upper and lower layers explicitly for each time step, reducing the CPU time in the computation. The computational region covered the Gulf of Mexico and the Caribbean Sea, as shown in Figure 2; the data were digitized with a spatial resolution of 2.5 km. The time step was changed to satisfy the stability condition, as explained in the following section.

The condition of the tsunami front is important for estimating the runup height and inundation area. In this study we used the moving boundary condition by employing the staggered leap-frog scheme, in which a water level and discharge are alternatively calculated. Assuming that a water level is al-

ready computed at each computation cell, we can compare the levels of the water surface and the bottom of the next landward cell. If the water level is higher than the latter, the water may flow into the lowland cell, meaning that a runup of tsunami proceeds.

Stability condition

Nonlinear terms in the momentum equation and the interactions between the two layers make it difficult to derive a stability condition using the Von Neumann method (e.g., Imamura, 1996). Moreover, the Courant-Friedrichs-Lewys (CFL) condition, which is normally used in the numerical scheme for wave propagation, is not directly applicable to the present case because a representative wave celerity (the phase velocity) cannot be uniquely determined. There are two celerities for progressive and reflected waves derived from the governing equation for two-layer flow. The analytical solution for linearized governing equations provides $C_1 = \sqrt{gh_1(1 + \alpha\beta)}$ and $C_2 = \sqrt{gh_2(1 - \alpha)/(1 + \alpha\beta)}$, where $\alpha = \rho_1/\rho_2$ and $\beta = h_2/h_1$. A stability condition is determined by selecting some arbitrary spatial grid interval Δx and a time step Δt. According to the above solution, the model is shown to be stable up to a certain limit of $\Delta x/\Delta t$, which varies with α and β. For example, in the case of $\alpha = 0.5$ and $\beta = 4.0$, the celerity of the upper layer C_2 controls the stability criteria. However, for the case of $\alpha = 0.4$ and $\beta = 1.0$, C_1 controls the stability criteria. We cannot determine a stability condition a priori. At each numerical step, we need to compare the maximum value of C_1 and C_2 in order to derive the stability condition.

NUMERICAL RESULTS

We discuss, in succession, the behavior of the rim wave, the tsunami caused by the flow into and out of the crater (the crater-generated tsunami), and the propagation of the crater-generated tsunamis and landslide-generated tsunamis in the Gulf of Mexico.

Tsunami generation

Behavior of the rim wave. According to breaking wave criteria, the amplitude of the rim wave is estimated to be on the order of the mean shelf water depth (Dean and Dalrymple, 1991). In the near field for a centered wave system, the higher frequency components will be dispersed backward and the wave amplitude will decrease with distance traveled due to turbulence and bottom friction. In addition, the wave amplitude will also decrease as a function of $1/r$ (r is the distance from the center of the crater). We can use the Ursell parameter ($= A\lambda^2/h^3$, where A is amplitude, λ, wave length, and h is water depth) to estimate the importance of nonlinearity (the second term in equation 3) relative to dispersion effects (the fourth term in equation 3). As shown in Figure 3, the values for the Ursell parameters are O(10) at the edge of the platform and O(1/10) in the deep water. This indicates that the effect of nonlinearity is dominant on the platform, whereas the dispersion effect becomes significant in deep water. It further suggests that breaking in shallow water does not amplify the wave height. The amplitude of the rim wave would be ~10 m at the edge of the platform and of several meters in deep water 500 km from the impact center.

Receding and rushing waves. We used nonlinear long-wave theory with dispersion effects to simulate the movement of water on the Yucatan platform. As shown in Figure 3, the water depth above the Yucatan platform around the crater was much shallower than the crater depth. Therefore, the crater shape does not strongly affect tsunami generation; i.e., the flow rate into crater cavity does not depend on the depth of the crater, but depends on water depth of the Yucatan platform. In Figure 5, the results of a numerical simulation of water movement in and around the crater are shown. This numerical simulation demonstrates that the water movement generates the receding and rushing waves. The water that flowed into the crater cavity accumulates to the point where the crater cavity is overfilled, which then generates the rushing wave outward as this accumulation collapses. In Figure 6, we show the maximum height of the water levels at the center and rim of the crater, and the period of oscillation of the water movement. The maximum height achieved by the water column within the crater is dependent on the water depth above the Yucatan platform. We found that the amplitude and oscillation period of the wave going out of the crater is controlled by the depth of the shallow-water region surrounding the crater. The lower the inward flow velocity in the shallow-water region, the lower the wave height of the rushing wave and the longer the oscillation period. If the water depth of the Yucatan platform was 200 m at the end of the Maastrichtian, the wave height and period at the edge of the crater are estimated as 50 m and 10 h, respectively. We modeled the numerical simulation for the cases with different crater depths. As shown in Figure 6, the depth of the crater affects the period of the crater-generated tsunami, but affects minimally the wave height.

Tsunami propagation

Crater-generated tsunami. We obtained the wave amplitude and period of receding and rushing waves as a function of the crater size and the water depth around the crater (Fig. 6). Using these results as initial conditions, we simulated propagation of the tsunami across the Gulf of Mexico followed by coastal runup.

Numerical calculations indicate that the coastal region of North America was attacked by two types of tsunamis; a receding wave and a rushing wave (Fig. 7). No measurable wave was found ahead of the receding wave, which suggests that the rim wave must have dispersed quickly during propagation to the shore. The receding wave traveled across the entire gulf within 10 h after the impact. The Mimbral and Brazos River

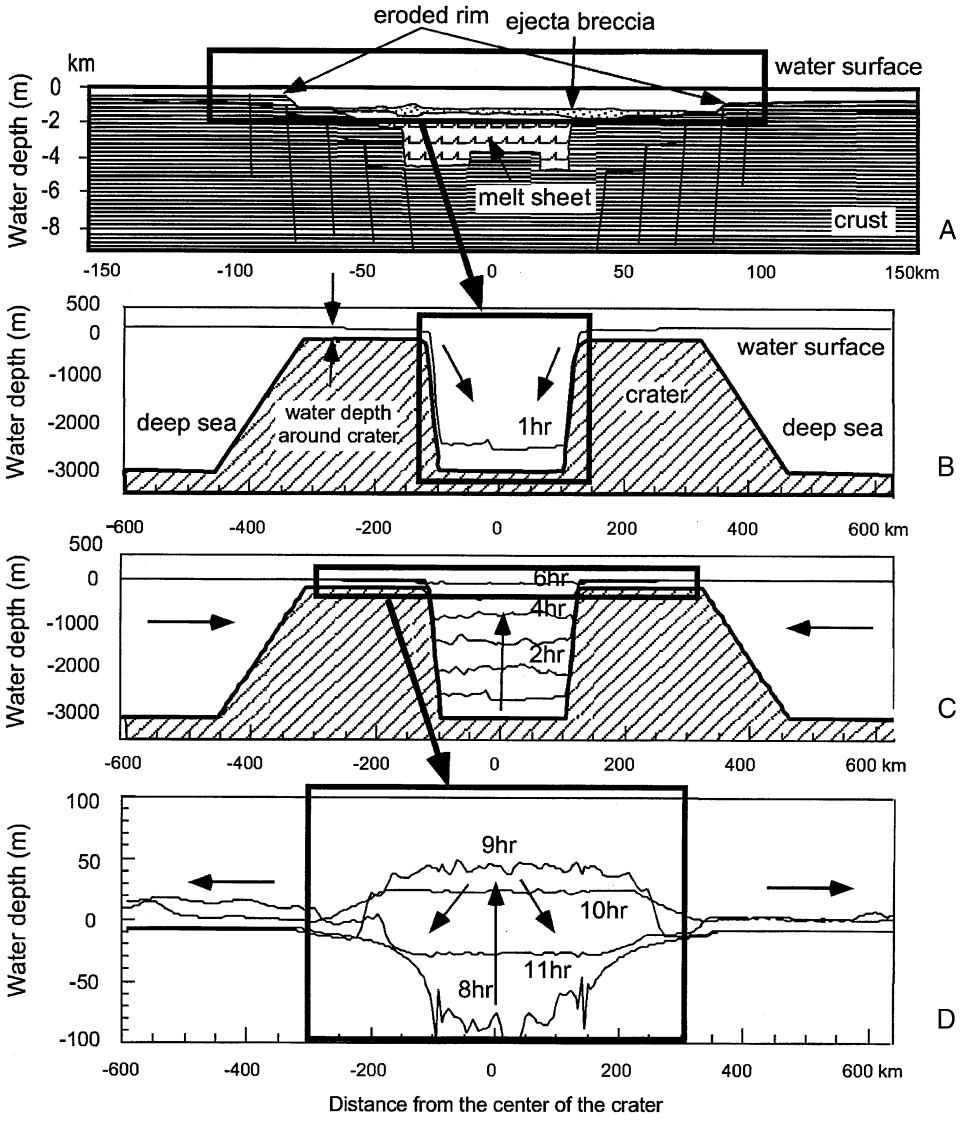

Figure 5. Time series of water mass movement flowing into and out of crater cavity. Because shallow-water region around crater strongly reduces inflow rate of water, it takes ~8 h to fill crater cavity for this case.

localities were exposed after ~10 h. The rushing wave, having a height of more than 200 m, then attacked the coast of North America and was reflected back, followed by significant wave oscillations having a periodicity of 1–2 h. Bourgeois et al. (1988) estimated the tsunami heights to have been 50–100 m high from the conditions requested for deposition of the K-T sandstone complex at the Brazos River, Texas, site. The wave height at the Brazos River locality in Figure 7 is consistent with this observation.

Calculations indicate that the tsunami runup inundated North America to 300 km beyond the Mississippi embayment (Fig. 8). The tsunami reached 300 m above sea level near the Rio Grande embayment, whereas the average runup height is in excess of 150 m.

Tsunami generated by landslide. We assume that a landslide occurred on the northern margin of the Yucatan platform just north of the impact point (Fig. 2). The location, size, and direction of the landslide are chosen arbitrarily. The area of the landslide is assumed to be 140 km (in east-west direction) by 75 km (in north-south direction). The thickness of the landslide layer along the north-south direction is assumed to be constant (100 m) for the southern region (0–20 km) and to decrease linearly toward the north (75–20 km). The landslide is assumed to be moving due north. We could simulate other cases, but in this chapter we just show the results for the parameters chosen to compare with the case of the crater-generated tsunami.

In the coastal regions of North America, the amplitude of the tsunami generated by a landslide is shown to be much smaller than that of the crater-generated tsunami (Fig. 9; cf. Fig. 7). However, the amplitude is highly dependent on the thickness of the sliding layer. If the layer were 10 times thicker than that assumed in this study, as suggested by Hildebrand (1997), the amplitude of the tsunami generated by the landslide is shown to be much larger and closer to that for the crater-

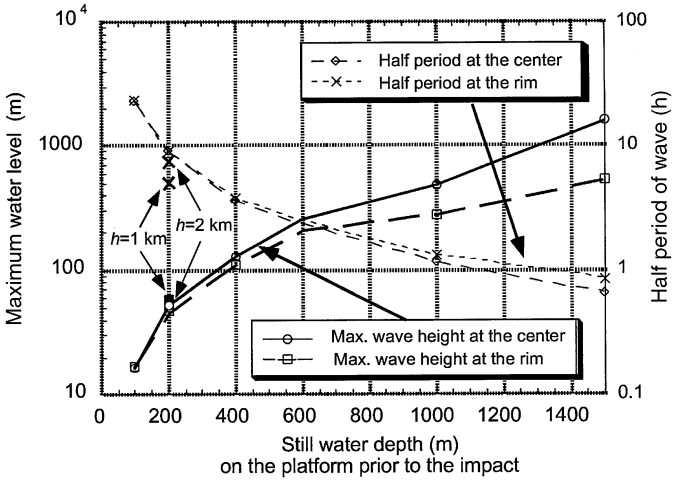

Figure 6. Relation of maximum water level, period of crater-generated tsunami at center and rim of crater, and still water depth of Yucatan platform. Numerical results for different crater depth models are also shown.

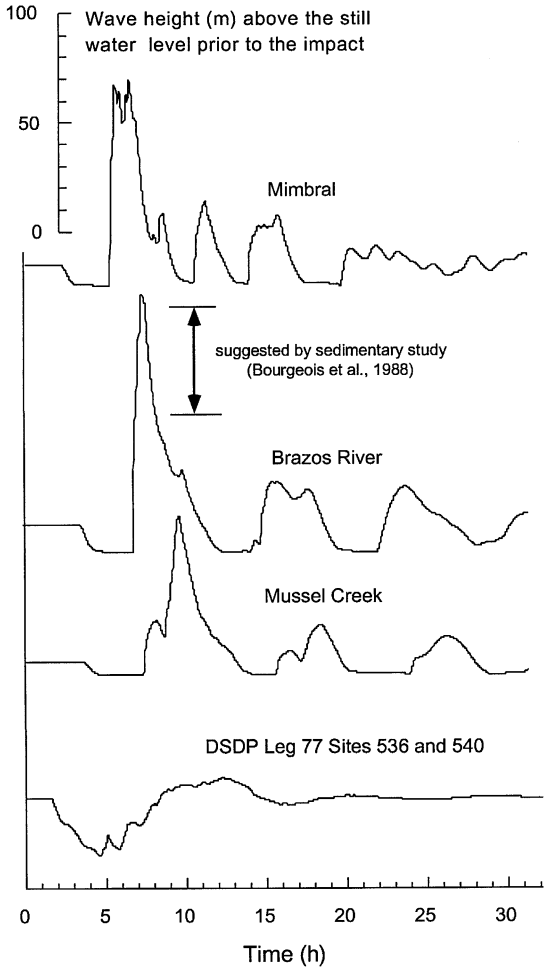

Figure 7. Temporal variations of water surface level at several locations in and around Gulf of Mexico for crater-generated tsunami. DSDP is Deep Sea Drilling Project.

generate tsunami; however, the first arrival in this case is a positive wave. This is the most significant difference between the crater-generated tsunami and the landslide-generated tsunami.

CONCLUSIONS

The wave height of the crater-generated tsunami is dependent on the depth of water covering the Yucatan platform at that time (Fig. 6), although the depth is difficult to estimate exactly. In this study we assumed that the depth of water was 200 m on the Yucatan platform, although the depth might have been much shallower. If the water was only 100 m deep, the maximum water level attained in the crater is reduced to ~40% of the maximum obtained for the 200 m case (Fig. 6). The energy of a wave is proportional to the square of the amplitude of that wave. Therefore, the magnitude of the tsunami for the 100 m case would be roughly ~17% that of the 200 m case, and the height of tsunami waves in costal regions would be 40% of the 200 m case.

Our calculations indicate there are significant differences between the crater-generated tsunamis and the landslide-generated tsunamis (cf. Figs. 7 and 9). This applies to their amplitudes in coastal regions as well as their directions and attenuations. The landslide-generated tsunami produces a rushing wave (first arrival), whereas the crater-generated tsunami produces a receding wave. This might be reflected in paleocurrent directions in the K-T sandstone complexes around the Gulf of Mexico (e.g., Smit et al., 1996). It is interesting to note that the study of the Moncada Formation in Cuba (Tada et al., this volume) suggests a receding wave as the first arrival.

Another contrasting feature of the two types of tsunami is that the amplitude of the crater-generated tsunami attenuates, whereas that of the landslide-generated tsunami does not attenuate. This is because the crater-generated tsunami runs up over the plain around the Gulf of Mexico, thus undergoing significant attenuation. In contrast, the landslide-generated tsunami is too small to run up, and thus undergoes little attenuation.

The magnitude of a landslide-generated tsunami is highly dependent on the area and thickness of the landslide. A seismic survey of the slope of the Yucatan platform is necessary to determine the landslide parameters; with this information, the generation and propagation of landslide-generated tsunami can be modeled more precisely. It is important to study the sedimentation mechanisms of the deposits formed on the floor of the crater in order to help clarify the amount of water that entered the crater. The continuously cored drill hole into the Chicxulub impact crater planned by the International Continental Scientific Drilling Program will provide a unique opportunity to do this.

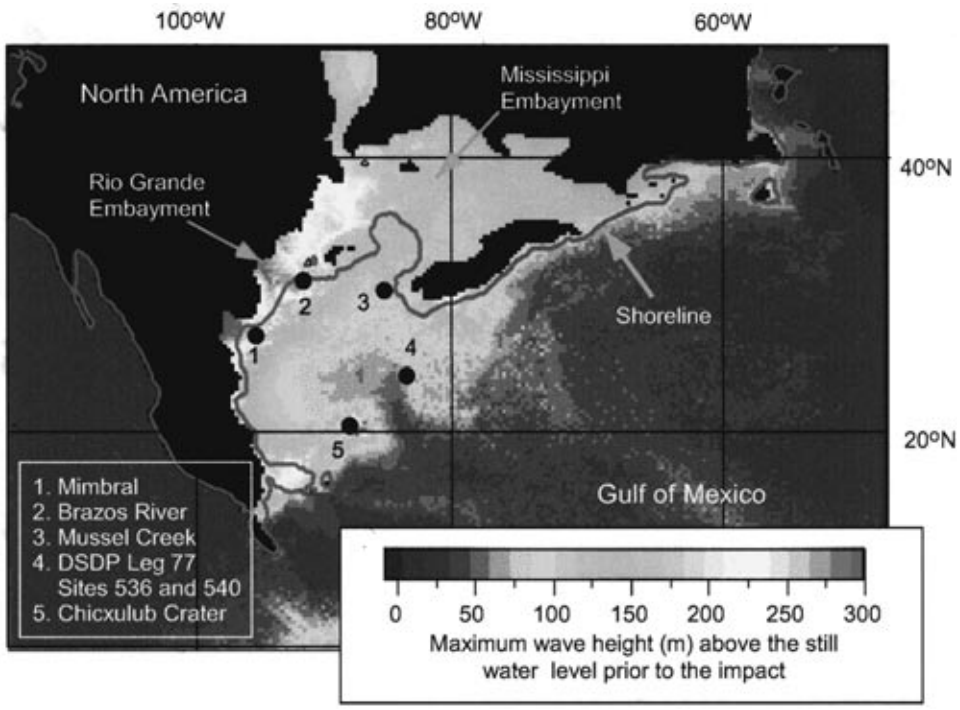

Figure 8. Inundation map of tsunami runup over plain around Gulf of Mexico. DSDP is Deep Sea Drilling Project.

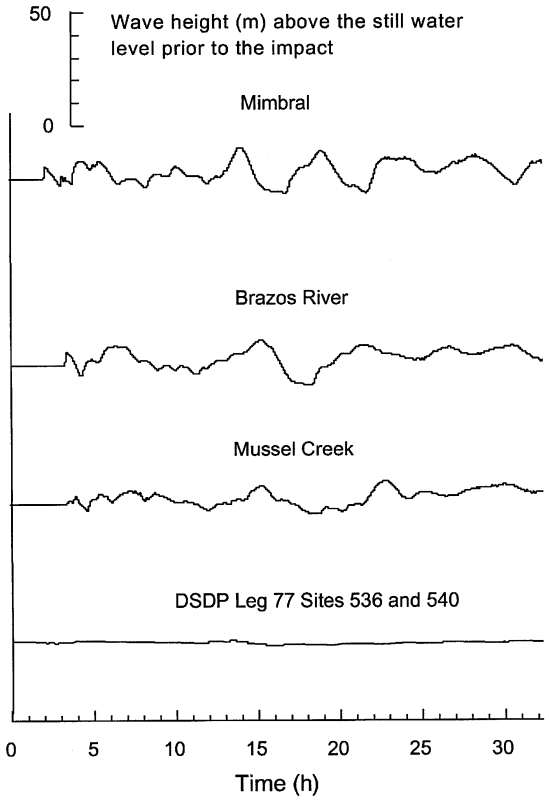

Figure 9. Temporal variations of water surface level at several locations in and around Gulf of Mexico for tsunami caused by landslide. DSDP is Deep Sea Drilling Project.

ACKNOWLEDGMENTS

We appreciate the critical comments and suggestions of A.R. Hildebrand, B. Simonson, and W.U. Reimold. We thank A.L. Moore for his efforts in improving our English, and the editor C. Koeberl for his helpful suggestions and efforts in handling the manuscript. This study was partially supported by grant-in-aids for scientific research of the Japan Society for the Promotion of Science (no. 11691116) and by research funds donated to University of Tokyo by I. Okawa, M. Iizuka, and K. Ihara.

REFERENCES CITED

Alvarez, L.W., Alvarez, W., Asaro, F., and Michel, H.V., 1980, Extraterrestrial cause for the Cretaceous-Tertiary extinction: Science, v. 208, p. 1095–1108.

Bohor, B.F., 1996, A sediment gravity flow hypothesis for siliciclastic units at the K/T boundary, northeastern Mexico, *in* Ryder, G., Fastovsky, D., and Gartner, S., eds., The Cretaceous-Tertiary event and other catastrophes in Earth history: Geological Society of America Special Paper 307, p. 183–195.

Bourgeois, J., Hansen, T.A., Wiberg, P.L., and Kauffman, E.G., 1988, A tsunami deposit at the Cretaceous-Tertiary boundary in Texas: Science, v. 241, p. 567–570.

Cita, M.B., Camerlenghi, A., and Rimoldi, B., 1996, Deep-sea tsunami deposits in the eastern Mediterranean: New evidence and depositional models: Sedimentary Geology, v. 104, p. 155–173.

Crawford, D.A., and Mader, C., 1998, Modeling asteroid impact and tsunami: Science of Tsunami Hazards, v. 16, p. 21–31.

Dean, R.G., and Dalrymple, R.A., 1991, Water wave mechanics for engineers and scientists: Singapore: World Scientific, 353 p.

Gault, D.E., and Sonett C.P., 1982, Laboratory simulations of pelagic asteroidal impact: Atmospheric injection, benthic topography, and the surface wave radiation field, *in* Silver, L.T., and Schultz, P.H., eds., Geological implications of impacts of large asteroids and comets on the earth: Geological Society of America Special Paper 190, p. 69–92.

Hildebrand, A.R., 1997, Contrasting Chicxulub Crater structural models: What can seismic velocity studies differentiate?: Journal of Conference Proceedings, v. 1, p. 37–46.

Hildebrand, A.R., Penfield, G.T., Kring, D.A., Pilkington, M., Camargo, Z.A., Jacobsen, S.B., and Boynton, W.V., 1991, Chicxulub crater: A possible Cretaceous/Tertiary boundary impact crater on the Yucatán Peninsula, Mexico: Geology, v. 19, p. 867–871.

Hildebrand, A.R., Pilkington, M., Ortiz-Aleman, C., Chavez, R.E., Urrutia-Fucugauchi, J., Connors, M., Graniel-Castro, E., Camara-Z., A., Halpenny, I.A., and Nichaus, D., 1998, Mapping Chicxulub crater structure with gravity and seismic reflection data, *in* Grady, M.M., Hutchison, R., McCall, G.J.H., and Rothery, D.A., eds., Meteorites: Flux with time and impact effects: Geological Society [London] Special Publication 140, p. 153–173.

Hills, J.G., Memchinov, I.V., Popov, S.P., and Teterev A.V., 1994, Tsunami generated by small asteroid impacts, *in* Gehrels, T., ed., Hazards due to comets and asteroids: Tucson, University of Arizona Press, p. 779–789.

Imamura, F., 1996, Review of tsunami simulation with a finite difference method, *in* Yeh, H., Liu, P., and Synolakis, C., eds., Long-wave runup models: Singapore, World Scientific, p. 25–42.

Imamura, F., and Gica, E.C., 1996, Numerical model for wave generation due to subaqueous landslide along a coast: A case of the 1992 Flores tsunami, Indonesia: Science of Tsunami Hazards, v. 14, p. 13–28.

Imamura, F., and Imteaz, M.M.A., 1995, Long waves in two-layers: Governing equations and numerical model: Science of Tsunami Hazards, v. 13, p. 3–24.

Kiyokawa, S., Tada, R., Oji, T., Tajika, E., Nakano, Y., Goto, K., Yamamoto, S., Takayama, H., Toyoda, K., Rojas, R., Gracia, D., Iturralde-Vinent, M.A., and Matsui, T., 2000, More than 500m thick K/T boundary sequence: Cacarajicara formation, Western Cuba. Impact related giant flow deposits [abs.], in Catastrophic events and mass extinction: Impacts and beyond: Houston, Texas, Lunar and Planetary Institute, LPI Contribution No. 1053, p. 100–101.

Morgan, J.V., Warner, M., and the Chicxulub Working Group, 1997, Size and morphology of the Chicxulub impact crater: Nature, v. 390, p. 472–476.

Okusa, S., and Yoshimura, M., 1981, Possibility of submarine slope failure due to waves (in Japanese): Tokai University Bulletin, v. 14, p. 227–234.

Raney, D.C., and Butler, H.L., 1976, Landslide generated water wave model: Journal of Hydraulic Research Division, American Society of Civil Engineering, v. 102, no. HY9, p. 1269–1281.

Ross, M.J., and Scotese, C.R., 1988, A hierarchical tectonic model of the Gulf of Mexico and Caribbean region: Tectonophysics, v. 155, p. 139–168.

Smit, J., Roep, Th.B., Alvarez, W. Claeys, P., Grajales-Nishimura, J.M., and Bermudez, J., 1996, Coarse-grained, clastic sandstone complex at the K/T boundary around the Gulf of Mexico: Deposition by tsunami waves induced by the Chicxulub impact?, *in* Ryder, G., Fastovsky, D., and Gartner, S., eds., The Cretaceous-Tertiary event and other catastrophes in Earth history: Geological Society of America Special Paper 307, p. 151–182.

Sohl, N.F., Martinez, R.E., Salmeron-Urena, P., and Soto-Jaramillo, F., 1991, Upper Cretaceous, *in* Salvador, A. ed., The Gulf of Mexico Basin: Boulder, Colorado, Geological Society of America, Geology of North America, v. J, p. 205–244.

Takayama, H., Tada, R., Matsui, T., Iturralde-Vinent, M.A., Oji, T., Tajika, E. Kiyokawa, S., Garcia, D., Okada, H., Hasegawa, T., and Toyoda, K., 2000, Origin of the Peñalver Formation in northwestern Cuba and its relation to K/T boundary impact event: Sedimentary Geology, v. 135, p. 295–320.

Ward, S.N., and Asphaug, E., 2000, Asteroid impact tsunami: A probabilistic hazard assessment: Icarus, v. 145, p. 64–78.

Manuscript Accepted by the Society March 22, 2001

Printed in the U.S.A.